



HAL
open science

Unlocking the potential of hydraulic fracturing flowback and produced water for CO₂ removal via mineral carbonation

Bizhou Zhu, Siobhan Wilson, Nina Zeyen, Maija Raudsepp, Ashkan Zolfaghari, Baolin Wang, Ben Rostron, Katherine Snihur, Konstantin von Gunten, Anna Harrison, et al.

► To cite this version:

Bizhou Zhu, Siobhan Wilson, Nina Zeyen, Maija Raudsepp, Ashkan Zolfaghari, et al.. Unlocking the potential of hydraulic fracturing flowback and produced water for CO₂ removal via mineral carbonation. *Applied Geochemistry*, 2022, 142, pp.105345. 10.1016/j.apgeochem.2022.105345 . hal-03869677

HAL Id: hal-03869677

<https://hal.science/hal-03869677>

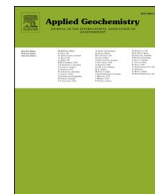
Submitted on 24 Nov 2022

HAL is a multi-disciplinary open access archive for the deposit and dissemination of scientific research documents, whether they are published or not. The documents may come from teaching and research institutions in France or abroad, or from public or private research centers.

L'archive ouverte pluridisciplinaire **HAL**, est destinée au dépôt et à la diffusion de documents scientifiques de niveau recherche, publiés ou non, émanant des établissements d'enseignement et de recherche français ou étrangers, des laboratoires publics ou privés.



Distributed under a Creative Commons Attribution - NonCommercial - NoDerivatives 4.0 International License



Unlocking the potential of hydraulic fracturing flowback and produced water for CO₂ removal via mineral carbonation

Bizhou Zhu^{a,*}, Siobhan A. Wilson^a, Nina Zeyen^a, Maija J. Raudsepp^a, Ashkan Zolfaghari^a, Baolin Wang^a, Ben J. Rostron^a, Katherine N. Snihur^a, Konstantin von Gunten^a, Anna L. Harrison^b, Daniel S. Alessi^a

^a Department of Earth and Atmospheric Sciences, University of Alberta, Edmonton, AB, Canada

^b Géosciences Environnement Toulouse, GET – CNRS – IRD – OMP – Université de Toulouse, 14, Avenue Edouard Belin, 31400, Toulouse, France

ARTICLE INFO

Editorial Handling by: Dr. Zimeng Wang

Keywords:

Mineral carbonation
Carbon mineralization
Hydraulic fracturing flowback and produced waters
Wastewater management
Carbon dioxide removal

ABSTRACT

Flowback and produced water (FPW) generated by hydraulic fracturing operations is highly saline and contains elevated concentrations of ions including calcium and magnesium. Here, we investigate the use of FPW as a source of calcium and magnesium for carbon dioxide (CO₂) removal and storage in carbonate minerals. We performed pH titration experiments to precipitate calcium and magnesium from three FPW samples from Alberta and Saskatchewan, Canada. Depending on the pH (8.5–12), calcite (CaCO₃) and brucite [Mg(OH)₂], with occasional aragonite (CaCO₃) and portlandite [Ca(OH)₂] precipitate from FPW within 24 h of exposure to atmospheric pCO₂ at ~18 °C. Our experiments demonstrate that pH adjustments are an effective means of precipitating calcium and magnesium carbonates and hydroxides from FPW, but that relying solely upon passive removal of CO₂ from air is limiting to carbonation. We estimate that carbonation of all calcium and magnesium from brines produced in conventional and hydraulic fracturing operations in Canada could store up to 1,010 Mt CO₂ annually. Carbonation rates could be improved by using higher pCO₂ gases, such as flue gases from fossil energy generation (via CO₂ capture), gas streams produced by Direct Air Capture plants or using novel looping technologies.

1. Introduction

Limiting anthropogenic climate warming to 1.5 °C requires a combination of energy efficiency, deep decarbonization, Carbon Dioxide Removal (CDR) from the atmosphere and Carbon Capture Utilization and Storage (CCUS) to reach net zero greenhouse gas (GHG) emissions by 2050 (IPCC, 2018). Mineral carbonation is a form of CDR, or CCUS (when using industrial CO₂ streams), that reacts alkaline Earth metals, such as Ca and Mg, with aqueous CO₂ to precipitate carbonate minerals (Gerdemann et al., 2007; Gislason et al., 2010; Harrison et al., 2013; Kelemen and Matter, 2008; Lackner et al., 1995; Park and Fan, 2004; Renforth et al., 2009; Schuiling and Krijgsman, 2006; Seifritz, 1990; Wilson et al., 2006, 2009, 2010). Sources of Ca and Mg for mineral carbonation can include alkaline wastes, such as mafic and ultramafic rocks and mine tailings (Assima et al., 2013, 2014; Harrison et al., 2013; Oskierski et al., 2013; Park and Fan, 2004; Pronost et al., 2012;

Renforth, 2019; Seifritz, 1990; Wilson et al., 2009, 2010), steel slag (Huijgen et al., 2005; Renforth, 2019), red mud (Renforth, 2012, 2019; Yadav et al., 2010), and cement (Fernández Bertos et al., 2004; Renforth et al., 2012; Xi et al., 2016). These feedstocks typically contain high abundances of Mg- and Ca-silicate minerals, that must first be dissolved to release the Ca and Mg for carbonate mineral formation (Power et al., 2013), and occasional lower abundances of Mg- and Ca-hydroxides and oxides that react readily with CO₂ under ambient conditions (Assima et al., 2013, 2014; Harrison et al., 2013; Hövelmann et al., 2012; Power et al., 2013; Pronost et al., 2012; Ruiz-Agudo et al., 2013; Wilson et al., 2010; Zhao et al., 2010). Chemical treatments, such as pH-swing methods (Park and Fan, 2004), are typically required to promote the dissolution of more recalcitrant silicate minerals and to improve conversion to carbonate minerals. As such, dissolution of feedstock minerals tends to be the rate-limiting step when using solid waste as feedstocks (Power et al., 2013). In addition, surface passivation of solid feedstocks,

* Corresponding author.

E-mail address: bizhou@ualberta.ca (B. Zhu).

¹ Present address: Department of Earth Sciences, University of Cambridge, Cambridge, United Kingdom.

non-ideal water saturation during reactions, and clogging of pore spaces due to rapid precipitation can hinder the efficiency of mineral carbonation in porous rock media (Harrison et al., 2015). These limitations can be circumvented by using an aqueous feedstock or hydroxide and oxide minerals that already contain highly reactive Mg and Ca.

Flowback and produced waters (FPW) are fluids produced from hydraulic fracturing wells by the oil and gas industry. FPW is a mixture of formation brine (>95 vol.%), hydraulic fracturing fluids, and dissolved rock constituents in the fracturing fluids (Alessi et al., 2017; Flynn et al., 2019; Folkerts et al., 2019; He et al., 2018; Lester et al., 2015; Stringfellow et al., 2014). Produced Waters (PW) from hydraulic fracturing wells are fracturing fluids that return to the surface at later stages during the production period. PW contain higher concentrations of total dissolved solids (TDS) and lower concentrations of organic constituents than FPW (Folkerts et al., 2019). PW also includes formation waters that are brought to the surface by conventional oil and gas wells (Rostron et al., 2002), and that have compositions close to those of subsurface formation brines. Herein, we refer to FPW as a collective term for wastewater that is produced by hydraulic fracturing wells, and we use PW for water that is generated by conventional oil and gas wells. Both FPW and PW contain elevated concentrations of Na and Cl, alkaline earth metals (e.g., Ca, Mg, and Sr), and transition metals (e.g., Mn and Zn) compared to freshwater (Alessi et al., 2017; Flynn et al., 2019; Folkerts et al., 2019; He et al., 2018; Lester et al., 2015; Rostron et al., 2002; Stringfellow et al., 2014; Zhong et al., 2019; Zolfaghari et al., 2016a). The alkaline earth metals in FPW are primarily sourced from dissolved carbonate minerals in host rocks (Harrison et al., 2017; Herz-Thyhsen et al., 2019). FPW has been identified to have sub-lethal effects and acute toxicity on aquatic animals; these effects are mainly attributed to the high TDS and the dissolved organic content of FPW (Folkerts et al., 2019, 2020; He et al., 2017; Weinrauch et al., 2021; Zolfaghari et al., 2016b). The compositions of FPW and PW vary from one geologic formation to another, across different locations within the same formation, and by production time, with large volumes of low-TDS water generated in the early stage of production and progressively higher-TDS water produced in the later stages until the solution chemistry represents that of the in-situ formation brine (Rostron et al., 2002; Zhong et al., 2019; Ziemkiewicz and He, 2015); nonetheless, the TDS of such waters is typically tens to thousands of times greater than the limit for agricultural irrigation (100s–1000s mg/L) (Canadian Council of Ministers of the Environment). Therefore, spills (Zhong et al., 2021) and improper disposal of FPW/PW are potentially detrimental to ecosystems and can affect surface water and groundwater systems.

Concentrations of Ca and Mg in FPW generated from hydraulic fracturing wells range from 10s to 10,000s ppm and 1s–1,000s ppm, respectively (Rostron et al., 2002; Zhong et al., 2019, 2021; Ziemkiewicz and He, 2015), which makes FPW/PW attractive resources for mineral carbonation. Druckenmiller and Maroto-Valer (2005) demonstrated rapid formation of calcite (CaCO₃) from initially acidic FPW samples under elevated temperature (75 °C and 150 °C) and pressure (41.4 bar and 103 bar) at a pH value of ~9 in experiments designed to simulate Carbon Capture and Storage (CCS) in a saline aquifer. Ferrini et al. (2009) proposed that the Mg in saline brines generated by desalination plants and hydraulic fracturing could be used for mineral carbonation under ambient conditions by reaction with high pCO₂ flue gases. They used synthetic, Mg-rich and Ca-poor brines to demonstrate precipitation of the hydrated Mg-carbonate mineral, nesquehonite (MgCO₃·3H₂O), under high salinity conditions.

In this study, we use FPW samples from a hydraulically fractured well and PW samples from a conventional well, from the Western Canadian Sedimentary Basin (WCSB), to evaluate the possibility of using Ca- and Mg-rich FPW and PW as feedstocks for mineral carbonation. Based on previously published analyses, these samples predominantly consist of formation water, and they contain minor amounts of hydraulic fracturing fluid additives (Folkerts et al., 2019; He et al., 2018; Rostron et al., 2002; Zhong et al., 2019). With the additives in FPW and PW and

their excess salinity, it can be challenging to model the aqueous speciation and the saturation indices (SI) of hypersaline fluids with respect to different minerals. Therefore, we have used benchtop experiments to adjust the initially acidic pH of FPW and PW samples and empirically assess which conditions are most favourable for precipitation of carbonate minerals at atmospheric pCO₂ and ambient temperature. We report detailed geochemical analyses of mineral precipitates and solution chemistry, and we assess the utility of thermodynamic modelling to predict the most suitable conditions for brine carbonation. Our experiments were designed to test conditions for storage sites and treatment plants for FPW and PW that could be built near water hubs in regions with active hydraulic fracturing operations. Based on our results, we provide estimates for the mineral carbonation potential of FPW and PW in Canada as well as guidance for design and optimization of industrial-scale carbonation of FPW, PW and other waste brines under ambient conditions.

2. Methodology

Three samples of FPW and one sample of PW were used as carbonation feedstocks. The FPW samples, FPW1a, FPW1b and FPW2, were collected from a single horizontally drilled and hydraulically fractured well in 2016 at 54° 28.9' N, 117° 10.4' W from the Duvernay Formation, Alberta, Canada. The PW sample (PW1), described as sample 'U of A 01–159B' by Rostron et al. (2002), was collected in 2001 at 49° 17.7' N, 102° 50.3' W from the Red River Formation in the Kingsford field, Saskatchewan, Canada. Table S1 provides a summary of the compositions and sources of these brine samples.

Prior to titration experiments, 300 mL of samples FPW1a and PW1 and 600 mL of samples FPW1b and FPW2 were filtered with Basix™ 0.22 µm polyethersulfone (PES) membranes to remove suspended particles and stored in polypropylene Nalgene® bottles. Aliquots (30 mL) of each filtered sample were titrated with 1.0 M NaOH to pH values between 8.5 and 12.0 (n = 8, in increments of 0.5 pH units; Table S1), which favors precipitation of carbonate and hydroxide minerals, in polypropylene containers using a Thermo Scientific Orion Star T910 Auto-titrator. Immediately following titration, all pH-modified brines were stirred at 50 rpm to react with atmospheric CO₂ at room temperature (18.0 ± 2.0 °C) for 24 hours. The electrical conductivity (EC) and pH of the four initial brines were measured immediately following the titration, and after the reaction was complete. Precipitates were separated from solutions after 24-hours of reaction and characterized using X-ray diffraction (XRD) and scanning electron microscopy (SEM) with energy dispersive X-ray (EDX) spectroscopy. Quantitative phase analysis with the Rietveld method (Bish and Howard, 1988; Hill and Howard, 1987; Rietveld, 1969) was done using XRD patterns. The elemental compositions of separated precipitates and brines were determined using inductively coupled plasma mass spectrometry (ICP-MS/MS). Equilibrium speciation modelling was done using PHREEQC version 3 (Parkhurst and Appelo, 2013) with the phreeqc.dat database, which has been recommended for modelling reactions in high ionic strength hydraulic fracturing brines (Haase et al., 2013). Please refer to Supplementary Information Section S2 for detailed information about experimental procedures and analytical methods.

3. Results and discussion

3.1. Evolution of solution chemistry

All the FPW and PW samples contained elevated concentrations of alkaline earth metals that form carbonate minerals. Initial elemental concentrations of the four brine samples are summarized in Table 1. Ca concentrations in untreated FPW1a, FPW1b, FPW2, and PW1 were 11,000 ± 100 ppm, 10,800 ± 290 ppm, 8180 ± 40 ppm, and 17,300 ± 310 ppm, respectively. Mg concentrations in FPW1a, FPW1b, FPW2 and PW1 were 793 ± 46 ppm, 841 ± 15 ppm, 699 ± 26 ppm and 1920 ±

Table 1

Initial pH, EC, DIC concentrations, and ion concentrations (ppm) in the original brines determined using ICP-MS/MS and ion chromatography (IC) analyses. Analytical uncertainties are given (in brackets). ICP-MS/MS and IC data are reported to 3 significant figures.

	FPW1a	FPW1b	FPW2	PW1	
pH	5.1	5.2	6.1	6.0	
EC (mS/cm)	205.1	220.5	189.2	231.7	
DIC (mg C/L)	0.79 (0.98)	2.45 (0.98)	2.30 (0.98)	2.31 (0.98)	
Major	Na	65800 (1500)	48000 (1000)	39500 (400)	91900 (2500)
	Ca	11000 (100)	10800 (290)	8180 (40)	17300 (310)
	Cl	139000 ^a	108000 (4500)	93600 (2500)	194000 ^a
Minor	Br	284 (5)	254 (6)	208 (8)	497(17)
	K	1940 (30)	1860 (50)	1630 (62)	4170 (70)
	Mg	793 (46)	841 (15)	699 (26)	1920 (110)
	Sr	1050 (30)	952 (16)	759 (20)	595 (11)
Trace	Al	<0.0429	4.70 (0.43)	4.71 (0.13)	<0.0384
	B	92.1 (1.8)	80.3 (1.3)	76.1 (0.1)	111 (2)
	Ba	3.20 (0.20)	3.11 (0.11)	3.37 (0.12)	14.9 (0.5)
	Cu	<0.488	<0.275	<0.266	0.0435 (0.0012)
	Fe	0.264 (0.008)	1.74 (0.02)	2.07 (0.06)	0.100 (0.002)
	Li	48.4 (1.0)	32.4 (0.3)	27.3 (0.3)	59.0 (0.6)
	Mn	4.37 (0.07)	4.37 (0.10)	1.68 (0.05)	0.195 (0.008)
	Ni	<0.572	<0.275	<0.266	<0.512
	P	<0.0458	BDL	BDL	<0.0411
	Pb	0.107 (0.001)	0.191 (0.001)	<0.178	0.0816 (0.0006)
	S	87.3 (2.7)	76.9 (2.4)	88.5 (0.3)	85.8 (6.9)
	Si	9.20 (1.10)	225 (6)	190 (3)	3.80 (0.10)
	Zn	0.734 (0.031)	<1.56	<1.51	1.05 (0.06)

^a Concentration measured with IC.

110 ppm, respectively.

The initial pH values of FPW1a, FPW1b, FPW2 and PW1 were 5.1, 5.2, 6.1, and 6.0, respectively (Table 1). The pH of all brines decreased by 0.5–1.0 units within 24 hours of mineral precipitation and completion of the titration experiments (Fig. S1B). Exceptions were observed for FPW1a and PW1 at pH 12.0: following titrations, the pH of FPW1a increased from 12.0 to 13.0 whereas that of PW1 remained constant at pH 12.0, even after 24 hours of reaction (Fig. S1B). The increase in pH for FPW1 and PW1 is likely attributed to an overshoot in NaOH addition during titration. The initial dissolved inorganic carbon (DIC) concentrations of FPW1a, FPW1b, FPW2, and PW1 were between 0.79 and 2.45 mg C/L (Table 1). The DIC concentrations of all pH-modified brines after 24 hours of reaction with air were still less than 10 mg C/L (Fig. S1C). No clear trend for DIC versus pH endpoint of titration was observed for any of the four brines. However, DIC reached a maximum value at pH 8.5 for FPW1a and FPW2 and decreased as the solutions were titrated to higher pH.

In general, the concentrations of both Ca and Mg decreased with increasing pH endpoint of titration after 24 hours of reaction with atmospheric CO₂ (Fig. 1). At a pH endpoint of 12.0, the Ca concentrations remaining in FPW1a, FPW1b, FPW2, and PW1 were 28.1%, 84.4%, 72.5% and 41.6% of that in the original brines, respectively. The greater magnitude of decrease in Ca concentrations in FPW1a and PW1 could be due to the overshoot in pH that was observed following titration (see Fig. S1).

Mg concentrations in the pH-modified brines after reaction for 24 hours remained at approximately the same level as the original brines when the pH endpoint values of titration were between 8.5 and 10.0, depending on the sample (Table 1 and Fig. 1). Mg concentrations decreased abruptly at pH endpoint values between 10.0 and 11.0 for most samples (i.e., FPW1a, FPW1b, FPW2) and between 8.5 and 10.0 for PW1. When the pH endpoint values for all samples were 11.0 or greater, the Mg concentrations after reaction with atmospheric CO₂ were below

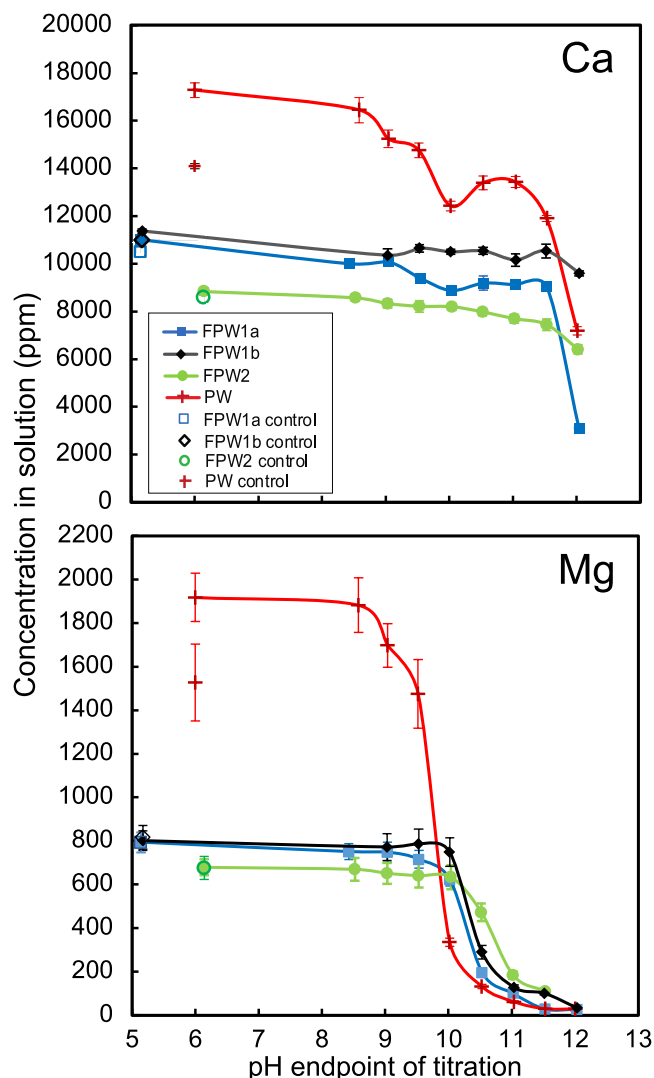


Fig. 1. Ca and Mg concentrations (ICP-MS/MS) of brine samples after reaction with atmospheric CO₂ for 24 hours as a function of pH endpoint of titration. The ionic concentrations of pH-modified brines and controls have been corrected for evaporative loss of water. The Ca and Mg concentrations of FPW1b and FPW2 are average values of duplicate samples. The error bars for Ca and Mg concentrations of FPW1a and PW1 are calculated based on standard deviation of ICP-MS/MS measurements. The error bars for FPW1b and FPW2 are the analytical error on each duplicate averaged, given as \pm one standard deviation. Error bars smaller than the labels are not shown.

the sample-specific detection limits of ICP-MS/MS measurements, which ranged from 84.5 to 90.0 ppm (Table S5). At those pH endpoint values, and accounting for analytical detection limits, less than 10.8% (FPW1a), 10.5% (FPW1b), 12.1% (FPW2), and 4.5% (PW1) of the Mg must have remained in solution (Table S5). Mg concentrations (Fig. 1) that are below the detection limits are plotted only intending to illustrate the trend of Mg concentration as a function of pH endpoint. The concentrations of other elements can be found in Table 1.

3.2. Mineralogy of precipitates

White, cloudy precipitates were first observed in all four brines when the pH endpoint of titration was between 9.0 and 9.5. Samples of the precipitates were recovered for the following experiments: pH 9.5–12.0 (FPW1a), pH 10.0–12.0 (FPW1b), pH 9.5–12.0 (FPW2) and pH 9.5–12.0 (PW1). The precipitates were analyzed with XRD Figs. 2 and S2 (Figs. 2 and S2) for mineral identification and quantitative phase analysis using

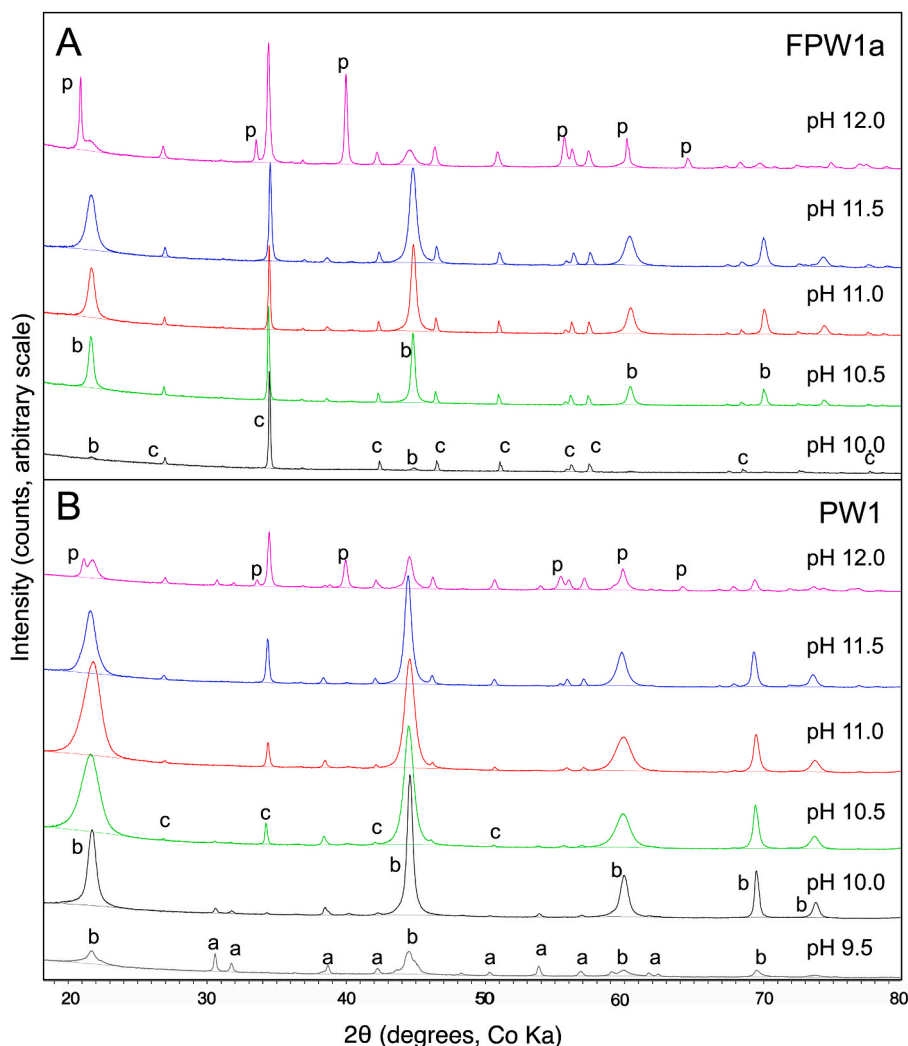


Fig. 2. XRD patterns for precipitates from (A) FPW1a and (B) PW1. a: aragonite (CaCO_3); b: brucite [$\text{Mg}(\text{OH})_2$]; c: calcite (CaCO_3); and p: portlandite [$\text{Ca}(\text{OH})_2$]. The most intense and diagnostic peaks of each phase are labelled at either the pH where they first appeared or where their abundance is greater than 10 wt.%.

Rietveld refinements (Table 2). Exceptions are the precipitates from FPW1a at pH 9.5, FPW1b at pH 10.0, and FPW2 at pH 9.5 and 10.0, which were only analyzed with SEM-EDX and/or qualitative XRD (Table 2), because it was not possible to perform phase quantification due to their very small mass ($\ll 1$ mg of precipitates per 30 mL of FPW). SEM images (Figs. 3–5) show aggregates of 1–3 μm subhedral to euhedral calcite rhombohedra, which are commonly coated in plates of brucite and portlandite with the occasional presence of a poorly crystalline Mg-silicate phase, possibly similar to kerolite [$\text{Mg}_3\text{Si}_4\text{O}_{10}(\text{OH})_2 \cdot n\text{H}_2\text{O}$] or stevensite [$(\text{M}_{2x}^+)(\text{Mg}_{3-x}\text{Si}_4\text{O}_{10}(\text{OH})_2 \cdot n\text{H}_2\text{O})$].

The precipitates that formed at pH 9.5 from FPW1a (Table 2, Figs. 3 and 4A) contain major amounts of calcite and trace amounts of brucite and a poorly crystalline Mg-silicate phase. At pH 9.5 in FPW2, both calcite and a poorly crystalline Mg-silicate phase were detected using XRD (Fig. S3). The precipitates formed at pH 9.5 from PW1 contain brucite, aragonite and a trace amount of calcite. Precipitates from FPW samples at pH 10.0–10.5 contain both calcite and brucite in varying abundances (Table 2). XRD results show that both calcite and brucite are present in precipitates at pH values between 10.0 and 12.0 FPW1a, FPW1b, and FPW2. In contrast, precipitates from PW1 at pH 9.5–11.5 also contain aragonite in addition to brucite and calcite. At pH 12.0, the precipitates from FPW1a are composed of calcite (43.5 wt.%), portlandite [$\text{Ca}(\text{OH})_2$] (28.3 wt.%) and brucite (28.2 wt.%), whereas the

precipitates from PW1 are composed of brucite (47.8 wt.%), calcite (28.1 wt.%), portlandite (16.8 wt.%) and aragonite (7.3 wt.%). Portlandite was not observed in precipitates generated from FPW1b or FPW2. Overall, the Rietveld refinement results (Table 2) show that phase abundance depends on both titration pH and brine chemistry.

Equilibrium speciation modelling using PHREEQC (Fig. S4) was performed to predict the SI of the original FPW1a brine titrated to endpoint pH values of 8.5–12.0, with respect to brucite, aragonite, calcite, portlandite, kerolite and other relevant minerals. The model results are consistent with laboratory observations of the precipitated phases during carbonation at ambient conditions. Notably, the difference between the modelled endpoint pH of titration, where $\text{SI} = 0$ (i.e., chemical equilibrium conditions) with respect to precipitated minerals, and the endpoint pH of titration where minerals precipitated in experiments, is typically between 0 and 1.5 pH units (see Section S3 of Supplementary Information for more detail).

3.3. Yield of Ca and Mg and the mass of CO_2 storage in precipitates

The mass of Ca and Mg (the ‘yield’) and the mass of CO_2 stored in the precipitates can be calculated using Eqs. (1)–(3), respectively:

$$\text{Ca yield} = \sum_{i=1}^n \left[\frac{\text{Ca}_i \times \% \text{phase}_i \times M_{\text{yield}}}{V_{\text{brine}}} \right] \quad (1)$$

Table 2
Yield of precipitates, mineralogy, and phase abundances following titration experiments.

Sample	pH	Yield (g/L)	Aragonite (wt.%)	Brucite (wt.%)	Calcite (wt.%)	Portlandite (wt.%)	Total (wt.%)	^a R _{wp} (%)
FPW1a	9.5	n/a ^b		t ^d	M ^d			
FPW1a	10.0	0.9		14.4	85.6		100.0	4.3
FPW1a	10.5	2.2		81.6	18.4		100.0	4.1
FPW1a	11.0	2.3		83.1	16.9		100.0	4.2
FPW1a	11.5	3.1		74.1	25.9		100.0	5.3
FPW1a	12.0	7.7		28.2	43.5	28.3	100.0	4.7
FPW1b-1	10.0	n/a ^b			M ^d			
FPW1b-2	10.0	n/a ^b			M ^d			
FPW1b-1	10.5	2.3		73.6	26.4		100.0	7.7
FPW1b-2	10.5	2.2		79.8	20.2		100.0	5.6
FPW1b-1	11.0	2.9		76.8	23.2		100.0	4.9
FPW1b-2	11.0	2.8		72.9	27.1		100.0	10.0
FPW1b-1	11.5	3.0		79.7	20.4		100.0	5.5
FPW1b-2	11.5	2.9		78.5	21.5		100.0	5.6
FPW1b-1	12.0	3.4		76.1	23.9		100.0	8.6
FPW1b-2	12.0	3.6		80.3	19.7		100.0	5.1
FPW2-1	9.5 ^c	n/a ^b			M ^d			
FPW2-1	10.0	0.2 ^b			M ^d			
FPW2-2	10.0	0.3 ^b			M ^d			
FPW2-1	10.5	0.3		54.9	45.1		100.0	7.3
FPW2-2	10.5	0.6		38.9	61.1		100.0	7.9
FPW2-1	11.0	1.3		77.6	22.4		100.0	6.0
FPW2-2	11.0	1.7		66.0	33.1		100.0	5.4
FPW2-1	11.5	2.3		69.7	30.3		100.0	5.2
FPW2-2	11.5	1.9		67.9	32.1		100.0	5.3
FPW2-1	12.0	2.8		62.2	37.8		100.0	4.8
FPW2-2	12.0	2.5		65.2	34.8		100.0	4.7
PW1	9.5	0.5	29.5	70.4	0.1		100.0	3.3
PW1	10.0	4.0	3.1	96.7	0.2		100.0	7.6
PW1	10.5	4.5	0.6	97.0	2.4		100.0	8.2
PW1	11.0	5.2	0.3	96.1	3.6		100.0	6.9
PW1	11.5	5.6	0.3	88.9	9.5	1.3	100.0	8.2
PW1	12.0	11.3	7.3	47.8	28.1	16.8	100.0	5.0

^a R_{wp} is the weighted pattern residual, a function of the least-squares residual, obtained by Rietveld refinement.

^b Precipitate samples were too small to conduct Rietveld refinement and, in cases where no value for yield is reported, too small to weigh without substantial sample loss.

^c A poorly crystalline to amorphous Mg-silicate phase was observed in this sample using SEM and/or XRD.

^d M denotes a major phase indicated by SEM and/or XRD when the samples were too small to conduct Rietveld refinements; t indicates a trace amount of phase.

$$\text{Mg yield} = \sum_{i=1}^n \frac{\text{Mg}_i \times \% \text{phase}_i \times M_{\text{yield}}}{V_{\text{brine}}} \quad (2)$$

$$\text{mass of CO}_2 \text{ stored} = \sum_{i=1}^n \left[\frac{\text{CO}_{2i} \times \% \text{phase}_i \times M_{\text{yield}}}{V_{\text{brine}}} \right] \quad (3)$$

where, Ca_i and Mg_i are the respective weight percent abundances of Ca and Mg in a given precipitate mineral, *i*, using its stoichiometric formula; CO_{2i} refers to weight percent abundance of CO₂ (in carbonate groups) in phase *i*; %*phase*_{*i*} is the abundance of phase *i*, as estimated using Rietveld refinement; *M*_{yield} (g) is the total mass of precipitates yielded during the experiments; and *V*_{brine} (L) is the volume of brine. The method we applied here assumes ideal endmember stoichiometry and that all phases are well crystallized. The calculated results for Ca and Mg yields and the mass of CO₂ sequestered are plotted as a function of pH endpoint of titration in Figs. S5 and 6, respectively.

The total yield of precipitates (mass of precipitates per unit volume of the solution) increases as a function of pH for all the brine samples (Table 2). For example, the total yield of precipitates in FPW1a doubled when the titration pH increased from 10.0 (0.9 g/L) to 10.5 (2.2 g/L) and is more than 8 times greater at pH 12.0 (7.7 g/L) than at pH 10.0. The first occurrence of large increases in the total yield of precipitates corresponds to the increasing production of brucite. Differences in total yield and the mineralogy of precipitates can be attributed to the amount of TDS, which decreases according to the order: PW1 > FPW1a > FPW1b > FPW2 (Table 1). The total yield of precipitates at any given pH value followed the same trend. The second significant increase in total precipitate yield, which occurred between pH 11.5 and 12.0 in FPW1a

and PW1, was due to the precipitation of portlandite and calcite.

Overall, the yields of Ca and Mg in the precipitates increase with increasing pH (Fig. S5). The yield of Ca increases sharply (from ~0.5 g/L to ~2.5 g/L) between pH 11.5 and 12.0 in FPW1a and PW1 during precipitation of calcite and portlandite. Ca is precipitated between pH 10.0 and 12.0 during formation of calcite in FPW1b and FPW2. The yield of Mg sharply increases in the precipitates between pH 10.0 and 10.5 in FPW1a, FPW1b and FPW2 and from pH 9.5–10.0 in PW1. Among the studied brines, the yield of Mg shows a strong correlation with the original Mg concentration in the brine samples. PW1 has a higher Mg yield than FPW1a, FPW1b and FPW2. In contrast, the yield of Ca in precipitates has no correlation with the initial Ca concentration in the brines. Caution is called for when using Rietveld refinement results to assess the mass balance for Ca, Mg, and CO₂ in solid samples because XRD data provide only an indirect description of crystal chemistry (Wilson et al., 2006). As such, fourteen precipitate samples (Table S6) were digested in acid for ICP-MS/MS analysis to further examine their elemental compositions. XRD and acid digestion results for Ca and Mg abundances are in agreement (Fig. S6). Thus, Eq. (3) can be used to provide an accurate estimate of CO₂ removal from air provided all of the precipitate can be recovered to measure yield with an analytical balance. The amount of CO₂ stored by precipitates (Fig. 6A, Eq. (3)) is almost entirely controlled by calcite precipitation, as calcite is the only carbonate phase in precipitates. Maximum values for CO₂ removal from air were obtained at pH 12: 1.46 g CO₂/L (FPW1a), 0.34 g CO₂/L (FPW1b), 0.42 g CO₂/L (FPW2), and 1.76 g CO₂/L (PW1). If the hydroxide minerals (brucite and portlandite) in precipitates were completely converted to carbonate minerals (nesquehonite and calcite/aragonite) via exposure to atmospheric CO₂ or a higher *p*CO₂ gas

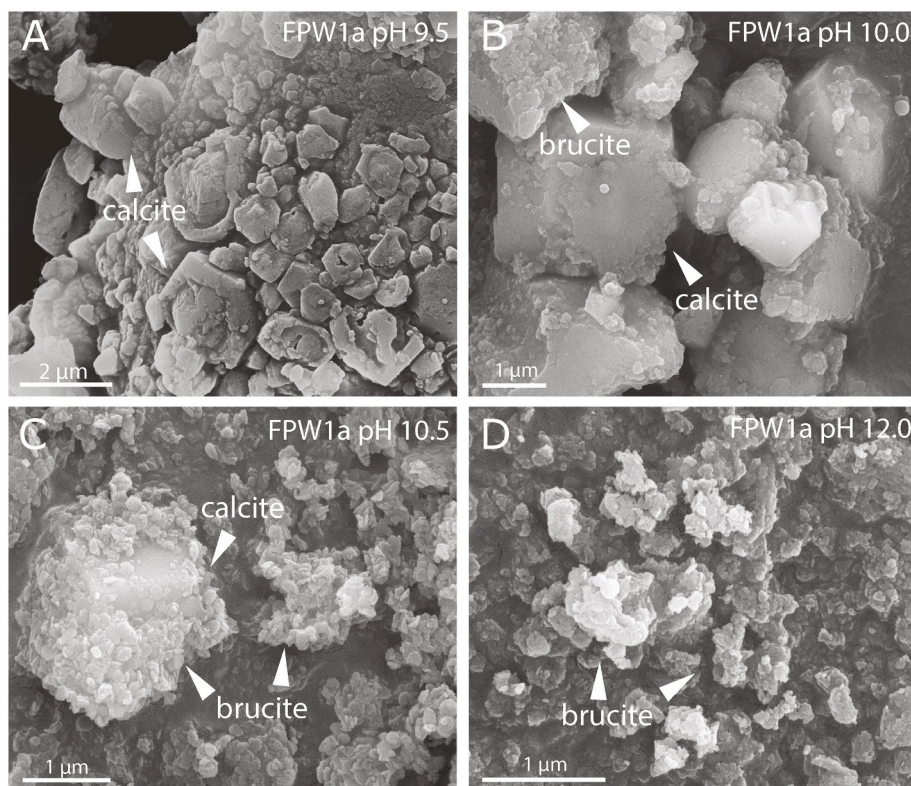


Fig. 3. Secondary electron SEM images of the precipitates from FPW1a at (A) pH 9.5, (B) pH 10.0, (C) pH 10.5, and (D) pH 12.0.

stream, the mass of CO₂ stored by precipitates (Fig. 6B) would increase to 4.38 g CO₂/L (FPW1a), 2.43 g CO₂/L (FPW1b), 1.69 g CO₂/L (FPW2), and 6.98 g CO₂/L (PW1) at pH 12.0.

Similar trends are observed when ICP-MS/MS results for Ca and Mg removal from solution are used (Fig. 6C) for the estimation of the CO₂ sequestration potential of precipitates. The CO₂ sequestration potential of precipitates would reach 10.1 g CO₂/L (FPW1a), 3.34 g CO₂/L (FPW1b), 3.81 g CO₂/L (FPW2), and 14.5 g CO₂/L (PW1) at pH 12.0 if the removed Ca and Mg can be carbonated to calcite/aragonite and nesquehonite, respectively. It should be noted that the CO₂ sequestration potential estimated based on Ca and Mg removal with ICP-MS/MS results (Fig. 6C) is at least 2-fold that estimated based on precipitates with XRD results (Fig. 6B), which is likely due to the partial loss of Ca-carbonate or hydroxide precipitate during separation of solid and solution through centrifugation. Thus, XRD results should be used only to determine mineralogy and the extent of carbonation, whereas ICP-MS/MS results should be used to measure the amount and efficiency of Ca and Mg removal from solution. Finally, if all the Ca and Mg in the four brines were carbonated, the maximum amount of CO₂ that can be sequestered is: 13.5 g CO₂/L (FPW1a), 12.2 g CO₂/L (FPW1b), 10.9 g CO₂/L (FPW2), and 22.5 g CO₂/L (PW1) (horizontal lines in Fig. 6C). Thus, with optimization, the mass of CO₂ removed from air using FPW and PW1 might be increased by 1–2 orders of magnitude.

3.4. CO₂ dissolution rate limits carbonation of brines

Our experimental results show that Mg-hydroxide (brucite) was preferentially precipitated from brines instead of hydrated Mg-carbonate minerals at alkaline pH. We conducted thermodynamic modelling (Fig. S4) using the initial solution composition of FPW1a as the input parameters and using model pH values between pH 5.0–13.0 to assess whether the mineralogy of precipitates obtained in our study can be reproduced. The starting DIC value (0.79 ± 0.98 g C/L) used for modelling was measured from untreated FPW1a in contact with atmospheric pCO₂ at room temperature (18 ± 2 °C). Model results show that

the FPW1a solutions at pH 5.0–13.0 were undersaturated with common hydrated Mg-carbonate minerals produced during mineral carbonation at low temperatures [dypingite, Mg₅CO₄(OH)₂·~5H₂O; hydromagnesite, Mg₅(CO₃)₄(OH)₂·4H₂O; and nesquehonite, MgCO₃·3H₂O], owing to the low concentration of DIC (Table 1 and Fig. S1C) in the initial solution and after titration. Although magnesite (MgCO₃) and disordered dolomite [CaMg(CO₃)₂] reach supersaturation, we did not observe those phases because their nucleation is kinetically inhibited at room temperature although it can be catalyzed using carboxyl functional groups on abiological substrates or microbial cell walls (McCutcheon et al., 2016; Power et al., 2017; Saldi et al., 2009).

FPW1a solutions at elevated pH are saturated with respect to both aragonite and calcite, which is consistent with the observed mineralogy of the precipitates, although aragonite was only observed in precipitates from PW1 (Table 2). The lack of aragonite in precipitates from FPW samples and the variation in abundance of Ca-carbonates might be attributed to the combined effects of instantaneous supersaturation and the aqueous Mg/Ca ratio (De Choudens-Sánchez and Gonzalez, 2009): (1) the PW1 sample (0.18) exhibited a higher molar Mg/Ca ratio than the FPW samples (0.12–0.14), which likely resulted in the co-existence of aragonite and calcite in PW1 precipitates; (2) as the level of calcite supersaturation increased in PW1 with increasing pH, calcite became more abundant (Table 2). In addition, the presence of organic additives in FPW samples may also have contributed to variations in carbonate mineralogy between PW and FPW samples. The formation of portlandite [Ca(OH)₂] is predicted from geochemical modelling (Fig. S4) at pH 12 and above, as was observed for FPW1a and PW1.

The nanoscale morphology of hexagonal platelets and rosettes of both brucite (e.g., Fig. 3C, D and 5A) and portlandite crystals (e.g., Fig. 5C) reflects rapid precipitation, as do the broad diffraction peaks observed for these phases in XRD patterns (Figs. 2 and S2). Although this morphology should provide a large reactive surface area for carbonation reactions (Fernández Bertos et al., 2004; Harrison et al., 2015), our results show that at pH > 10.5 (FPW1a, FPW1b and FPW2) and pH > 9.5 (PW1) precipitates contain a greater abundance of hydroxide phases

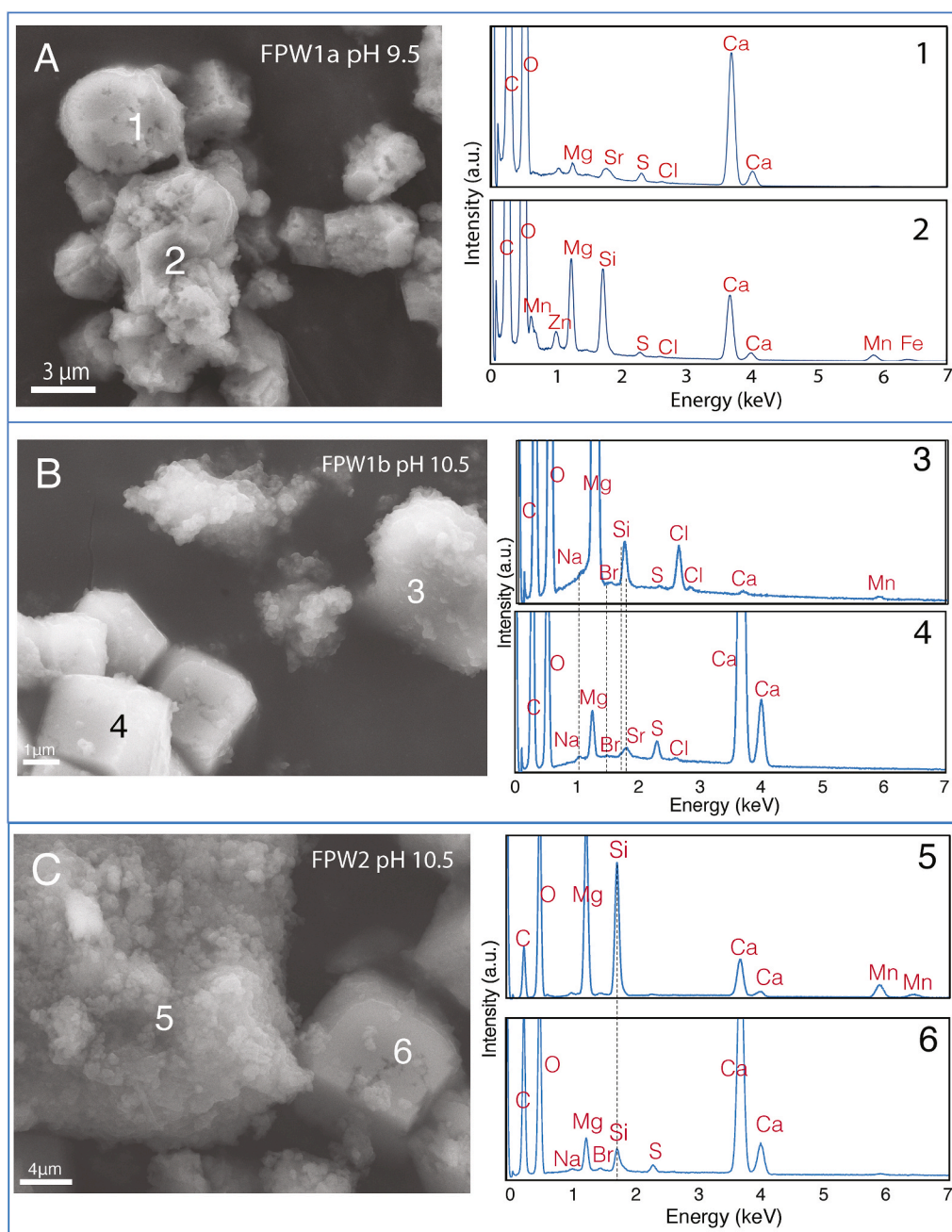


Fig. 4. (A) Secondary electron SEM image of the precipitates in FPW1a at pH 9.5: (1) EDX spectrum indicates S- and Sr-bearing calcite and brucite mixture; (2) EDX spectrum of a mixture of brucite, a Mg-silicate and trace amounts of Mn, Fe, and Zn, which are likely associated with (hydr)oxide phase(s). (B) Secondary electron SEM image showing morphology of precipitate minerals from FPW1b at pH 10.5: (3) EDX spectrum of a mixture of brucite, a Mg-silicate phase and halite; (4) EDX spectrum of S- and Sr-bearing calcite. (C) Secondary electron SEM image of precipitates from FPW2 at pH 10.5: (5) EDX spectrum of a mixture of brucite, a Mg-silicate phase, calcite with either Mn incorporation into one or more of these minerals and/or the presence of a Mn-(hydr)oxide phase; (6) EDX spectrum of S-bearing calcite and a lesser amount of a Mg-silicate phase.

than carbonate phases (Table 2). The rapid precipitation of reactive brucite and portlandite indicates that hydroxide mineral precipitation outpaces the dissolution of atmospheric CO_2 into brines. Carbon limitation in this system can likely be overcome by promoting the dissolution of CO_2 gas and increasing DIC concentration using a concentrated supply of high $p\text{CO}_2$ gas (Harrison et al., 2013; Wilson et al., 2010) while maintaining elevated pH conditions through addition of basic solutions. We therefore propose that carbonation of brines using higher $p\text{CO}_2$ gas streams should be explored. The greatest yield of Ca and Mg, and the greatest CO_2 sequestration, are likely to be achieved within one of two pH intervals, provided elevated pH is maintained: (1) within the pH range of 9.5–10.0 (FPW1a, FPW1b, and FPW2), where Ca-carbonate minerals (aragonite or calcite) are most favoured to form over portlandite and brucite or (2) at $\text{pH} > 10.5$ (FPW1a, FPW1b, FPW2, and PW1) where nanocrystalline hydroxide minerals [brucite (Harrison et al., 2013; Wilson et al., 2010; Zhao et al., 2010) and/or portlandite

(Ruiz-Agudo et al., 2013)] are most favoured to form but would require further carbonation using higher CO_2 -concentration gases with a greater mineral/water ratio. The latter strategy has potential to utilize the full carbonation potential of the brine by carbonating Mg as well as Ca; however, a greater amount of base is needed to achieve this outcome and further modifications need to be made to maximize the CO_2 sequestration capacity. It should be noted that the exact pH ranges for these reactions will possibly depend on the ionic strength of a specific brine. Future experiments are needed to systematically test the impacts of ionic strength on the extent and nature of mineral precipitation. The expense and embodied carbon involved in using NaOH to achieve the desired pH will also need to be considered as part of a Life Cycle Assessment (LCA) and Techno-Economic Analysis (TEA).

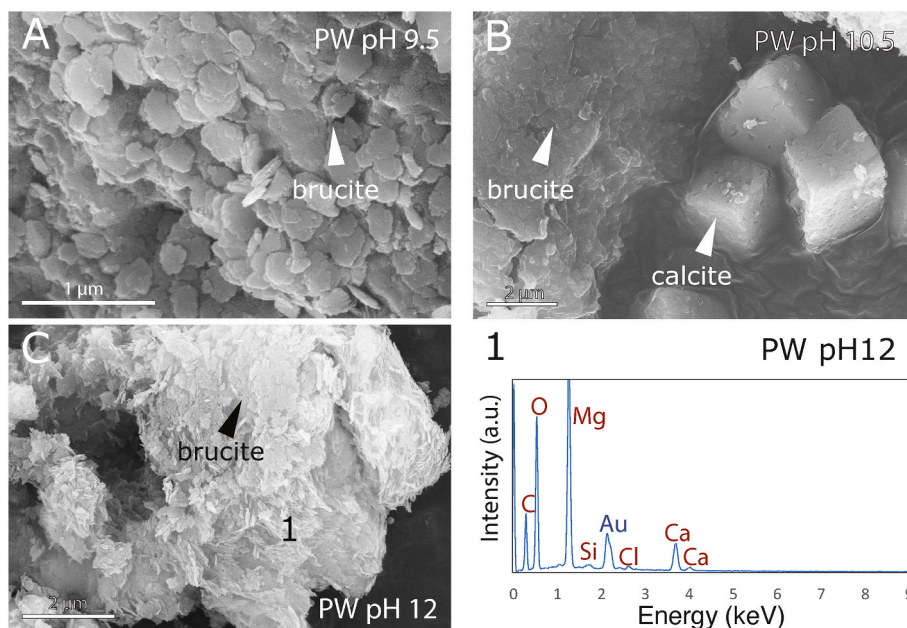


Fig. 5. Secondary electron SEM images of the precipitates from PW1 at (A) pH 9.5, (B) pH 10.5, and (C) pH 12.0. The samples are coated with gold (labelled in blue on the EDX spectrum). (For interpretation of the references to colour in this figure legend, the reader is referred to the Web version of this article.)

3.5. Prospects for implementation of brine carbonation in the oil and gas sector

Oil and gas operations including extraction, processing, and distribution were directly responsible for ~5.2 Gt CO₂ equivalent (CO₂e) emissions in 2018, which is ~15% of total global emissions (International Energy Agency, 2018). The Canadian oil and gas sector was directly responsible for 191.4 Mt CO₂e of emissions in 2019 and the transportation sector, which is fueled predominantly by oil and gas, contributed another 185.8 Mt CO₂e, representing 52% of the 730 Mt CO₂e emitted nationally (Environment and Climate Change Canada, 2021). Traditional CCS associated with enhanced oil and gas recovery currently stores ~260 Mt CO₂e worldwide every year (Global CCS Institute, 2019). With >36 Gt CO₂e emitted per year globally (Friedlingstein et al., 2019), achieving net zero GHG emissions by 2050 will likely require capturing CO₂ directly from air as well as from large point-sources of industrial CO₂ (Kelemen et al., 2020; McQueen et al., 2020; Sanz-Pérez et al., 2016).

Our results show that pH adjustment of waste brines can be used to activate precipitation of Ca/Mg-bearing minerals, including highly reactive brucite and portlandite, for CO₂ removal from air. Despite the environmental concerns about hydraulic fracturing (HF) activities and FPW production, the significant worldwide production of FPW makes it a good candidate feedstock for the mineralization and sequestration of atmospheric CO₂. Kondash et al. (2017) estimated that a typical hydraulically fractured well produces a median volume of 1700–14,300 m³/year of FPW during its first 5–10 years of operation. We estimated that 66.8 million m³ of FPW were produced in Canada during 2020 from the 16,068 registered hydraulic fracturing wells that were drilled after 1990 in the Western Canadian Sedimentary Basin (WCSB). Unconventional oil and gas production in the United States is estimated to have produced 803 million m³ of hydraulic fracturing fluids within the past 6–10 years (Kondash and Vengosh, 2015). We estimate that hydraulically fractured wells in the United States generated 356.4 million m³ of FPW in 2019 alone. In China, it is estimated that a total of 2.16 million m³ of FPW were generated from the Fuling shale gas field in the Sichuan Basin between 2014 and 2015. With the recent surge in shale gas exploration in China (Liu et al., 2018; Qin et al., 2017), it is predicted

that the gas fields in the Sichuan Basin will generate 20–55 million m³/year of FPW from 2020 to 2030 (Zou et al., 2018), and production is expected to further increase as more gas fields are developed.

In this study, we created a comprehensive well library of more than 850,000 HF and conventional wells registered in Canada by combining data in the GeoScout, AccuMap, and FracFocus databases. FracFocus was used to identify HF wells, and GeoScout and AccuMap were used to extract well production data such as FPW production rate and water chemistry data (i.e., Ca and Mg concentrations). Accounting for wells drilled after 1990, there are 16,871 HF and 127,631 conventional wells with reported production data. The concentrations of both Ca and Mg in FPW for wells in the WCSB range between 500 and 70,000 mg/L. For HF wells, the median concentrations for Ca and Mg are 1780 mg/L and 650 mg/L, respectively. For conventional wells, the median concentration values for Ca and Mg are 1330 mg/L and 435 mg/L, respectively.

Based on the volumetric production of FPW estimated in this study, and the results of our titration experiments, we estimate the carbonation capacity of hydraulic fracturing brine for the USA, Canada and China based on (1) observed precipitate yields (using our XRD data), (2) precipitate mineralogy (using our XRD data) and (3) total brine Ca and Mg concentrations (using our ICP-MS data). Although we did not precipitate (hydrated) Mg-carbonate minerals from our experiments, brucite is well known to carbonate easily at ambient conditions (1) by reaction with atmospheric CO₂ in mine tailings and (2) by reaction with simulated flue gas in both slurries and water undersaturated conditions (Wilson et al., 2010, 2014; Harrison et al., 2013; Turvey et al., 2018; Hamilton et al., 2020). As such, we include the CO₂ storage capacity of Mg in this estimation. Adjusting the pH of all the brines produced in one year to 10.5–12.0, and reacting them for 1 day with ambient CO₂ in air, could readily store 4.70–31.7 kT (WCSB, Canada; 2019), 52.7–355 kT (US, 2019), and 0.319–2.15 kT (Fuling shale, China, 2014–2015) of CO₂ based on the amount of carbonate minerals obtained in our experiments (Fig. 6A), where the lower and upper ends of each range depend on the pH endpoint of titration. If a comparable amount of hydroxide minerals observed in our experiments can be precipitated and then fully converted to carbonate minerals (Fig. 6B), the CO₂ storage capacity can be enhanced to 59.3–123 kT (WCSB, Canada; 2019), 665–1380 kT (US, 2019) and 4.03–8.36 kT (Fuling shale, China; 2014–2015). When we use

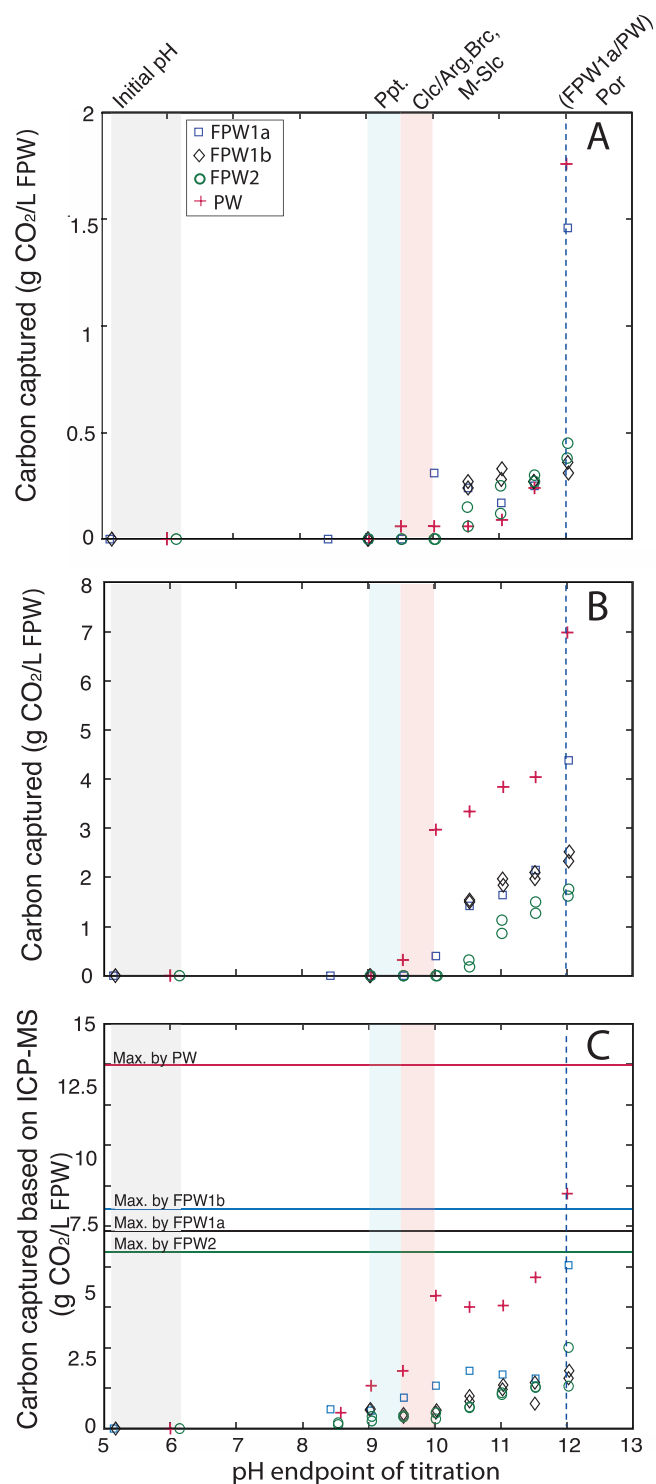


Fig. 6. (A) Observed mass of CO₂ stored (estimated using XRD data). (B) Mass of CO₂ that can be sequestered by fully carbonating precipitates (estimated using XRD data). (C) Mass of CO₂ that can be sequestered by carbonating Ca and Mg removed from solution (estimated using ICP-MS/MS data). Horizontal blue (FPW1a), black (FPW1b), green (FPW2), and red (PW) lines plot the maximum CO₂ sequestration potential of the brines. (For interpretation of the references to colour in this figure legend, the reader is referred to the Web version of this article.)

the more accurate ICP-MS results from our experiments to estimate how much Ca and Mg were removed, and assume all of the brucite will be converted to carbonates (Fig. 6C), the CO₂ storage capacity reaches 117–252 kT (WCSB, Canada; 2019), 1310–2830 kT (US, 2019) and 7.94–17.1 kT (Fuling shale, China; 2013–2014). These values do not account for how much CO₂ could be mineralized with optimization of the process and they do not reflect the maximum CO₂ sequestration potential of FPW, which is much greater.

Assessing the maximum CO₂ sequestration potential of a feedstock for mineralization, or of any other CDR or other CCUS technology, is crucial to determine whether or not a proposed technology could be brought to Gt scale and is thus worth pursuing. These initial estimates must then be followed by LCA and TEA. We have sufficient data to make an estimate for the maximum CO₂ sequestration potential of FPW in Canada, but further work is needed to make similar estimates for China and the USA. Herein, estimates of maximum CO₂ sequestration potential are based on the monthly volumetric data for FPW production in Canada in combination with water chemistry data, which allow us to calculate the annual production of aqueous Ca and Mg by mass from typical HF and conventional wells. HF wells typically generate more Ca and Mg than conventional wells during the first year of production, an average of 8420 kg of Ca and 3075 kg of Mg for HF wells, and 3535 kg of Ca and 1155 kg of Mg for conventional wells. Accounting for wells drilled after 1990, HF wells in Canada generate approximately 142 Mt of Ca and 51.8 Mt of Mg annually, and conventional wells generate 451 Mt of Ca and 147.5 Mt of Mg each year (see Section S2.7 in the Supplementary Information). If all the Ca and Mg produced by FPW in Canada can be carbonated to calcite/aragonite and nesquehonite, respectively, FPW produced by HF wells could store approximately 250 Mt of CO₂ annually, and the wastewater produced from conventional wells in Canada can store approximately 762 Mt of CO₂ each year. Accordingly, we estimate that the CO₂ sequestration potential of FPW in Canada could be equivalent to 1,010 Mt. If our estimates are accurate, and if it were possible to fully utilize this potential, it would fully offset the annual CO₂ emissions from not only oil and gas production and processing (~191 Mt CO₂e in 2019) (Environment and Climate Change Canada, 2021) but all of Canada's GHG emissions. The estimated carbonation potential of FPW in Canada has a value of 50.6 billion CAD given the national price (Government of Canada) of 50 CAD per tonne of CO₂ in 2022. A more comprehensive estimation of the CO₂ storage potential of FPW in China, the United States and other countries is needed to assess the full scale of this resource and to understand the economic implications of its use. Importantly, additional base would need to be added to precipitate all of the Ca and Mg from FPW. This base (NaOH) would likely need to be produced at scale using electrochemical methods. Access to the full CO₂ sequestration capacity of FPW would require maintenance of solution pH above a critical value to continually precipitate carbonate minerals and hydroxides while simultaneously removing the precipitate from solution to drive continued precipitation. Whether this is feasible at scale remains to be assessed using LCA and TEA.

The only industries that are, or could become, large enough to utilize the Mt or Gt of carbonate minerals this would produce are construction and CDR with looping technologies. Carbonate products of CCUS are already being used as construction materials (Hills et al., 2020; Di Maria et al., 2020). CO₂ removal using FPW could also be combined with Ca and Mg looping technologies. Unlike other mineralization CO₂ removal technologies, looping reuses Ca and Mg by first allowing portlandite and brucite to react with atmospheric CO₂, then calcining the resultant Ca- and Mg-carbonates to obtain a high pCO₂ gas stream that can be stored underground (Kelemen et al., 2020; McQueen et al., 2020). These steps are repeated in a loop so that each mole of Ca or Mg can be used to remove many moles of CO₂ from the atmosphere, rather than locking a single mole of CO₂ permanently into a carbonate mineral. Several recent studies have proposed that Ca and Mg looping methods could be used to scale-up the carbon storage capacity of limited natural or industrial feedstocks for mineral carbonation (Kelemen et al., 2020; McQueen

et al., 2020), such that the technology might be scaled to the Gt CO₂ per year level. The Ca and Mg resource present in FPW and PW might be used in such a looping plant (Fig. 7). In this scenario, the pH-modified FPW would serve as an aqueous sorbent and the precipitated Ca- and Mg-hydroxides or carbonates could be combined with Ca (e.g., Fan et al., 2018; Keith et al., 2018; Manovic and Anthony, 2011) and Mg (e.g., Hwang et al., 2018; Jin et al., 2019; Kelemen et al., 2020; McQueen et al., 2020; Siriwardane and Stevens, 2009; Tuan and Lee, 2018) looping technologies for further extraction of concentrated CO₂. The purified CO₂ from calcination could then (1) be transported using the growing network of CO₂ pipelines (e.g., the Alberta Carbon Trunk Line in the WCSB) for injection into geologic formations dedicated to storage or (2) be utilized in the manufacture of value-added products (Kelemen et al., 2020; McQueen et al., 2020). Finally, the MgO and CaO calcination products could be reused in the looping process to scavenge more CO₂ from air. Unlike most of the previously developed looping systems (e.g. Fan et al., 2018; Hwang et al., 2018; Jin et al., 2019; Siriwardane and Stevens, 2009), in which mineral carbonation happens at elevated temperature and pressure conditions, both the initial carbonate mineral precipitation and reuse of MgO and CaO calcination products could take place at ambient conditions as proposed by Kelemen et al. (2020) and McQueen et al. (2020); however, further work would be needed to assess rates of CO₂ removal under climatic conditions in the WCSB. Using waste brines as a source of Mg and Ca for looping technologies may also be a preferable alternative to calcining magnesite, dolomite, and limestone, thus maintaining permanent storage of the CO₂ already found in these highly stable mineral deposits.

3.6. Uncertainties for implementation at larger scale

While this first estimation of the annual CO₂ sequestration potential of Ca and Mg in conventional and hydraulic fracturing flowback water suggests huge potential for CO₂ removal, it should not be neglected that this process needs further assessment and refinement before a transition from laboratory experiments to the pilot and commercial scales can be contemplated. For example, removal of suspended materials as was done in our study, for instance through micro-scale filtration, might not be cost-effective on the commercial level; therefore, the influence of suspended materials on mineral precipitation should be considered. Flynn et al. (2019) identified that suspended solids (>0.22 μm) in FPW contain aragonite, calcite, muscovite, quartz, and sanidine. The occurrence of pre-existing calcite and aragonite could be beneficial as it is likely to

promote heterogeneous precipitation of more Ca-carbonates (e.g., Aguiar et al., 2003). Adding calcite seeds into a solution that is saturated with respect to calcite increases the precipitation rate while adding quartz seeds increases the nucleation rate (Lioliou et al., 2007). Although the above evidence demonstrates a catalytic behavior of suspended particles, the effects of pre-existing muscovite and sanidine or a combination of different minerals on carbonate precipitation remains unclear and needs further investigation.

The organic matter in hydraulic fracturing fluids may cause uncertainty in the prediction of CO₂ removal. Pearson et al. (2020) showed that peat-derived dissolved organic matter (DOM) slightly inhibits the efficiency of Ca extraction via calcite precipitation (<10%) between 0.17 and 15.70 mg C/L DOM. Various organic compounds may incorporate into or sorb onto calcite surfaces (e.g., Ramseyer et al., 1997; Lee et al., 2005; Pearson et al., 2020), which may affect the quality of precipitated carbonate minerals if they are to be utilized by the construction industry. Further research is needed to investigate the effect of organic compounds in FPW on the rate of carbonate precipitation and the efficiency of CO₂ sequestration in minerals. Nonetheless, our results show that the pH values at which different minerals precipitate from FPW are predictable using geochemical modelling simply by knowing the inorganic solution chemistry: we successfully predicted precipitation of minerals within 0–1.5 pH units regardless of the presence of organic matter.

4. Conclusions

The results of our research confirm, for the first time, the proposal of Ferrini et al. (2009) and demonstrate that real FPW can be utilized for CO₂ removal at ambient conditions. The precipitates from conventional produced water and FPW contain Ca-carbonates (aragonite and calcite), Ca-hydroxide (portlandite) and Mg-hydroxide (brucite) depending on the adjusted pH and/or Ca/Mg ratio of the initial brine. The Ca in FPW is readily carbonated whereas the Mg precipitated in brucite requires further carbonation. Despite the high ionic strength of the FPW samples, PHREEQC modeling with the phreeqc.dat database was used to successfully predict the mineralogy of precipitates. This style of modelling could therefore be applied to support design and optimization of industrial-scale FPW carbonation reactions. Therefore, we included both Ca and Mg to estimate the maximum annual CO₂ sequestration potential of conventional produced water and FPW in Canada. The CO₂ sequestration potential of brines in Canada alone is huge. If a cost effective and

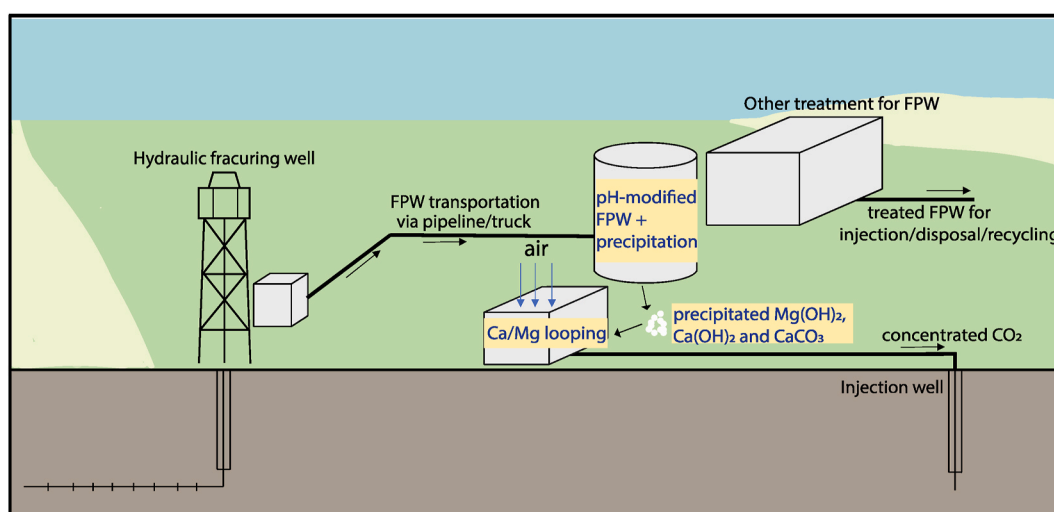


Fig. 7. Schematic illustration of FPW carbonation via CDR coupled to Ca/Mg looping plus injection into a sedimentary formation (not drawn to scale). The design of the installation is based on publicly accessible information on hydraulic fracturing operations (Alessi et al., 2017), wastewater treatment plants (US U.S. EPA and U.S. Environmental Protection Agency, 2020), and looping methods (McQueen et al., 2020; Kelemen et al., 2020).

environmentally sustainable strategy is found to supply base for this process, brine carbonation could have a multi-Gt CO₂ removal potential globally.

Author contributions

BZ designed and conducted the experiments, collected and analyzed XRD, ICP-MS/MS and SEM data, conducted geochemical modelling, interpreted the data and wrote the manuscript. SAW provided the idea for the project, designed the experiments, facilitated XRD and SEM data collection and analyses, and participated in data interpretation and writing. NZ and MR contributed to SEM data collection and interpretation and facilitated geochemical modelling. AZ contributed to data collection, interpretation, and estimation of CO₂ sequestration potential. BW facilitated collection of ICP-MS/MS data. BJR collected samples and contributed to data interpretation. KNS and KvG facilitated ICP-MS/MS data collection and analysis. ALH contributed to geochemical modelling. DSA contributed samples, ICP-MS/MS data collection, geochemical modelling, and data interpretation.

Declaration of competing interest

The authors declare that they have no known competing financial interests or personal relationships that could have appeared to influence the work reported in this paper.

Acknowledgements

BZ was supported by an Ian McLaren Cook Sr Graduate Scholarship from the University of Alberta. Funding for this project was provided by the Canada Research Chairs Program and through a Natural Sciences and Engineering Research Council of Canada (NSERC) Discovery and Accelerator Supplement to SAW as well as by a NSERC Collaborative Research and Development to DSA. We thank J. Cheng and J. Janzen from the Environmental Economic Geology Laboratory for their assistance with data acquisition. We thank N. Gerein (FE-SEM), K. Nichols and R. Funk (XRD) and M. Labbe (experimental set up) from the Department of Earth and Atmospheric Sciences at the University of Alberta for their technical support. We thank Associate Editor Yuanzhi Tang for expert editorial handling and three anonymous reviewers for their comments that greatly improved the quality of this manuscript.

Appendix A. Supplementary data

Supplementary data to this article can be found online at <https://doi.org/10.1016/j.apgeochem.2022.105345>.

References

- Aguar, R., Muhr, H., Plasari, E., Burty, M., Rocabo, P., 2003. Comparative study of the influence of homogeneous and heterogeneous (multi-phase) precipitation processes on the particle size distribution. *Chem. Eng. Technol.* 26 (3), 292–295. <https://doi.org/10.1002/ceat.200390044>.
- Alessi, D., Zolfaghari, A., Kletke, S., Gehman, J., Allen, D.M., Goss, G.G., 2017. Comparative analysis of hydraulic fracturing wastewater practices in unconventional shale development: water sourcing, treatment, and disposal practices. *Can. Water Resour. J.* 42 (2), 105–121. <https://doi.org/10.1080/07011784.2016.1238782>.
- Assima, G.P., Larachi, F., Beaudoin, G., Molson, J., 2013. Dynamics of carbon dioxide uptake in chrysotile mining residues - effect of mineralogy and liquid saturation. *Int. J. Greenh. Gas Control* 12, 124–135. <https://doi.org/10.1016/j.ijggc.2012.10.001>.
- Assima, G.P., Larachi, F., Molson, J., 2014. Emulation of ambient carbon dioxide diffusion and carbonation within nickel mining residues. *Miner. Eng.* 59, 39–44. <https://doi.org/10.1016/j.mineng.2013.09.002>.
- Bish, D.L., Howard, S.A., 1988. Quantitative phase analysis using the Rietveld method. *J. Appl. Crystallogr.* 21, 86–91.
- Canadian Council of Ministers of the Environment, 15 June 2021. https://ccme.ca/en/chemical/215#_ag_irrigation_concentration.
- De Choudens-Sánchez, V., Gonzalez, L.A., 2009. Calcite and aragonite precipitation under controlled instantaneous supersaturation: elucidating the role of CaCO₃ saturation state and Mg/Ca ratio on calcium carbonate polymorphism. *J. Sediment. Res.* 79 (6), 363–376. <https://doi.org/10.2110/jsr.2009.043>.
- Di Maria, A., Snellings, R., Alaerts, L., Quaghebeur, M., Van Acker, K., 2020. Environmental assessment of CO₂ mineralisation for sustainable construction materials. *Int. J. Greenh. Gas Control* 93, 102882. <https://doi.org/10.1016/j.ijggc.2019.102882>.
- Druckemiller, M.L., Maroto-Valer, M.M., 2005. Carbon sequestration using brine of adjusted pH to form mineral carbonates. *Fuel Process. Technol.* 86 (14–15), 1599–1614. <https://doi.org/10.1016/j.fuproc.2005.01.007>.
- Environment and Climate Change Canada, 2021. National Inventory Report 1900–2019: Greenhouse Gas Sources and Sinks in Canada. Environment and Climate Change Canada. https://publications.gc.ca/collections/collection_2021/eccc/En81-4-2019-1-eng.pdf. (Accessed 16 November 2020).
- Fan, Y., Yao, J.G., Zhang, Z., Sceats, M., Zhuo, Y., Li, L., Maitland, G.C., Fennell, P.S., 2018. Pressurized calcium looping in the presence of steam in a spout-fluidized-bed reactor with DFT analysis. *Fuel Process. Technol.* 169, 24–41. <https://doi.org/10.1016/j.fuproc.2017.09.006>.
- Fernández Bertos, M., Simons, S.J.R., Hills, C.D., Carey, P.J., 2004. A review of accelerated carbonation technology in the treatment of cement-based materials and sequestration of CO₂. *J. Hazard Mater.* 112 (3), 193–205. <https://doi.org/10.1016/j.jhazmat.2004.04.019>.
- Ferrini, V., Vito, C.D., Mignardi, S., 2009. Synthesis of nesquehonite by reaction of gaseous CO₂ with Mg chloride solution: its potential role in the sequestration of carbon dioxide. *J. Hazard Mater.* 168, 2–3. <https://doi.org/10.1016/j.jhazmat.2009.02.103>.
- Flynn, S.L., von Gunten, K., Warchola, T., Snihr, K., Forbes, T.Z., Goss, G.G., Gingras, M.K., Konhauser, K.O., Alessi, D.S., 2019. Characterization and implications of solids associated with hydraulic fracturing flowback and produced water from the Duvernay Formation, Alberta, Canada. *Environ. Sci.: Process. Impacts* 21, 242–255. <https://doi.org/10.1039/c8em00404h>.
- Folkerts, E.J., Blewett, T.A., Delompré, P., Mehler, W.T., Flynn, S.L., Sun, C., Zhang, Y., Martin, J.W., Alessi, D.S., Goss, G.G., 2019. Toxicity in aquatic model species exposed to a temporal series of three different flowback and produced water samples collected from a horizontal hydraulically fractured well. *Ecotoxicol. Environ. Saf.* 180, 600–609. <https://doi.org/10.1016/j.ecoenv.2019.05.054>.
- Folkerts, E.J., Heuer, R.M., Flynn, S., Stieglitz, J.D., Benetti, D.D., Alessi, D.S., Goss, G.G., Grosell, M., 2020. Exposure to hydraulic fracturing flowback water impairs mahimahi (*Coryphaena hippurus*) cardiomyocyte contractile function and swimming performance. *Environ. Sci. Technol.* 54, 13579–13589. <https://doi.org/10.1021/acs.est.0c02719>.
- Friedlingstein, P., Jones, M.W., O'Sullivan, M., Andrew, R.M., Hauck, J., Peters, G.P., Peters, W., Pongratz, J., Sitch, S., Le Quéré, C., et al., 2019. Global carbon budget 2019. *Earth Syst. Sci. Data* 11 (4), 1783–1838. <https://doi.org/10.1021/acs.est.0c02719>.
- Gerdemann, S.J., O'Connor, W.K., Dahlin, D.C., Penner, L.R., Rush, H., 2007. Ex situ aqueous mineral carbonation. *Environ. Sci. Technol.* 41, 2587–2593. <https://doi.org/10.1021/es0619253>.
- Gislason, S.R., Wolff-Boenisch, D., Stefansson, A., Oelkers, E.H., Gunnlaugsson, E., Sigurdardottir, H., Sigfusson, B., Broecker, W.S., Matter, J.M., Stute, M., Axelsson, G., Fridriksson, T., 2010. Mineral sequestration of carbon dioxide in basalt: a pre-injection overview of the CarbFix project. *Int. J. Greenh. Gas Control* 4, 537–545. <https://doi.org/10.1016/j.ijggc.2009.11.013>.
- Global CCS Institute, 2019. Global Status of CCS 2019: Targeting Climate Change. https://www.globalccsinstitute.com/wpcontent/uploads/2019/12/GCC_GLOBAL_STAT_US_REPORT_2019.pdf. (Accessed 15 June 2021).
- Government of Canada Website, 15 June 2021. <https://www.canada.ca/en/environment-climate-change/services/climate-change/pricing-pollution-how-it-will-work/industry/pricing-carbon-pollution.html>.
- Haase, C., Dethlefsen, F., Ebert, M., Dahmke, A., 2013. Uncertainty in geochemical modelling of CO₂ and calcite dissolution in NaCl solutions due to different modelling codes and thermodynamic databases. *Appl. Geochem.* 33, 306–317. <https://doi.org/10.1016/j.apgeochem.2013.03.001>.
- Hamilton, J.L., Wilson, S.A., Morgan, B., Harrison, A.L., Turvey, C.C., Paterson, D.J., Dipple, G.M., Southam, G., 2020. Accelerating mineral carbonation in ultramafic mine tailings via direct CO₂ reaction and heap leaching with potential for base metal enrichment and recovery. *Econ. Geol.* 115, 303–323. <https://doi.org/10.5382/econgeo.4710>.
- Harrison, A.L., Dipple, G.M., Power, I.M., Mayer, K.U., 2015. Influence of surface passivation and water content on mineral reactions in unsaturated porous media: implications for brucite carbonation and CO₂ sequestration. *Geochem. Cosmochim. Acta* 148, 477–495. <https://doi.org/10.1016/j.gca.2014.10.020>.
- Harrison, A.L., Jew, A.D., Dustin, M.K., Thomas, D.L., Joe-Wong, C.M., Bargar, J.R., Johnson, N., Brown, G.E., Maher, K., 2017. Element release and reaction-induced porosity alteration during shale-hydraulic fracturing fluid interactions. *Appl. Geochem.* 82, 47–62. <https://doi.org/10.1016/j.apgeochem.2017.05.001>.
- Harrison, A.L., Power, I.M., Dipple, G.M., 2013. Accelerated carbonation of brucite in mine tailings for carbon sequestration. *Environ. Sci. Technol.* 47, 126–134. <https://doi.org/10.1021/es3012854.b>.
- He, Y., Flynn, S.L., Folkerts, E., Zhang, Y., Ruan, D., Alessi, D.S., Martin, J.W., Goss, G.G., 2017. Chemical and toxicological characterizations of hydraulic fracturing flowback and produced water. *Water Res.* 114, 78–87. <https://doi.org/10.1016/j.watres.2017.02.027>.
- He, Y., Sun, C., Zhang, Y., Folkerts, E.J., Martin, J.W., Goss, G.G., 2018. Developmental toxicity of the organic fraction from hydraulic fracturing flowback and produced waters to early life stages of zebrafish (*Danio rerio*). *Environ. Sci. Technol.* 52, 820–830. <https://doi.org/10.1021/acs.est.7b06557>.
- Herz-Thyhsen, R.J., Kaszuba, J.P., Dewey, J.C., 2019. Dissolution of minerals and precipitation of an aluminosilicate phase during experimentally simulated hydraulic

- fracturing of a mudstone and a tight sandstone in the Powder River Basin, WY. *Energy Fuels* 33 (5), 3947–3956. <https://doi.org/10.1021/acs.energyfuels.8b04443>.
- Hill, R.J., Howard, C.J., 1987. Quantitative phase analysis from neutron powder diffraction data using the Rietveld method. *J. Appl. Crystallogr.* 20, 467–474.
- Hills, C.D., Tripathi, N., Carey, P.J., 2020. Mineralization technology for carbon capture, utilization, and storage. *Front. Energy Res.* 8, 1–14. <https://doi.org/10.3389/fenrg.2020.00142>.
- Hövelmann, J., Putnis, C.V., Ruiz-Agudo, E., Austrheim, H., 2012. Direct nanoscale observations of CO₂ sequestration during brucite [Mg(OH)₂] dissolution, 2012. *Environ. Sci. Technol.* 46 (9), 5253–5260. <https://doi.org/10.1021/es300403n>.
- Huijgen, W.J.J., Witkamp, G.J., Comans, R.N.J., 2005. Mineral CO₂ sequestration by steel slag carbonation. *Environ. Sci. Technol.* 39 (24), 9676–9682.
- Hwang, B.W., Lim, J.H., Chae, H.J., Ryu, H.J., Lee, D., Lee, J.B., Kim, H., Lee, S.C., Kim, J.C., 2018. CO₂ capture and regeneration properties of MgO-based sorbents promoted with alkali metal nitrates at high pressure for the sorption enhanced water gas shift process. *Process Saf. Environ. Protect.* 116, 219–227. <https://doi.org/10.1016/j.psep.2018.02.008>.
- International Energy Agency, 2018. World Energy Outlook 2018. Accessed June 2021. <https://www.iea.org/reports/world-energy-outlook-2018/oil-and-gas-innovation?language=zh#abstract>.
- IPCC (Intergovernmental Panel on Climate Change), 2018–2019. Global Warming of 1.5°C. An IPCC Special Report on the impacts of global warming of 1.5°C above pre-industrial levels and related global greenhouse gas emission pathways. In: The context of strengthening the global response to the threat of climate change, sustainable development, and efforts to eradicate poverty. https://www.ipcc.ch/site/assets/uploads/sites/2/2019/06/SR15_Full_Report_High_Res.pdf. (Accessed 16 November 2020).
- Jin, S., Ko, K.J., Lee, C.H., 2019. Direct formation of hierarchically porous MgO-based sorbent bead for enhanced CO₂ capture at intermediate temperatures. *Chem. Eng. J.* 371, 64–77. <https://doi.org/10.1016/j.cej.2019.04.020>.
- Keith, D.W., Holmes, G., St Angelo, D., Heidel, K., 2018. A process for capturing CO₂ from the atmosphere. *Joule* 2, 1573–1594.
- Kelemen, P.B., Matter, J., 2008. In situ carbonation of peridotite for CO₂ storage. *Proc. Natl. Acad. Sci. U. S. A.* 105, 17295–17300. <https://doi.org/10.1073/pnas.0805794105>.
- Kelemen, P.B., McQueen, N., Wilcox, J., Renforth, P., Dipple, G., Vankeuren, A.P., 2020. Engineered carbon mineralization in ultramafic rocks for CO₂ removal from air: review and new insights. *Chem. Geol.* 550, 119628. <https://doi.org/10.1016/j.chemgeo.2020.119628>.
- Kondash, A., Vengosh, A., 2015. Water footprint of hydraulic fracturing. *Environ. Sci. Technol. Lett.* 2 (10), 276–280. <https://doi.org/10.1021/acs.estlett.5b00211>.
- Kondash, A.J., Albright, E., Vengosh, A., 2017. Quantity of flowback and produced waters from unconventional oil and gas exploration. *Sci. Total Environ.* 574, 314–321. <https://doi.org/10.1016/j.scitotenv.2016.09.069>.
- Lackner, K.S., Wendt, C.H., Butt, D.P., Joyce, E.L., Sharp, D.H., 1995. Carbon dioxide disposal in carbonate minerals. *Energy* 20, 1153. [https://doi.org/10.1016/0360-5442\(95\)00071-N](https://doi.org/10.1016/0360-5442(95)00071-N).
- Lee, Y.J., Elzinga, E.J., Reeder, R.J., 2005. Cu(II) adsorption at the calcite-water interface in the presence of natural organic matter: kinetic studies and molecular-scale characterization. *Geochem. Cosmochim. Acta* 69, 49–61. <https://doi.org/10.1016/j.gca.2004.06.015>.
- Lester, Y., Ferrer, I., Thurman, E.M., Sitterley, K.A., Korak, J.A., Aiken, G., Linden, K.G., 2015. Characterization of hydraulic fracturing flowback water in Colorado: implications for water treatment. *Sci. Total Environ.* 512–513, 637–644. <https://doi.org/10.1016/j.scitotenv.2015.01.043>.
- Lioliou, M.G., Paraskeva, C.A., Koutsoukos, P.G., Payatakes, A.C., 2007. Heterogeneous nucleation and growth of calcium carbonate on calcite and quartz. *J. Colloid Interface Sci.* 308 (2), 421–428. <https://doi.org/10.1016/j.jcis.2006.12.045>.
- Liu, Q., Lei, Q., Xu, H., Yuan, J., 2018. China's energy revolution strategy into 2030. *Resour. Conserv. Recycl.* 128, 78–89. <https://doi.org/10.1016/j.resconrec.2017.09.028>.
- Manovic, V., Anthony, E.J., 2011. Integration of calcium and chemical looping combustion using composite CaO/CuO-based materials. *Environ. Sci. Technol.* 45 (24), 10750–10756. <https://doi.org/10.1021/es202292c>.
- McCutcheon, J., Wilson, S.A., Southam, G., 2016. Microbially accelerated carbonate mineral precipitation as a strategy for in situ carbon sequestration and rehabilitation of asbestos mine sites. *Environ. Sci. Technol.* 50 (3), 1419–1427. <https://doi.org/10.1021/acs.est.5b04293>.
- McQueen, N., Kelemen, P., Dipple, G., Renforth, P., Wilcox, J., 2020. Ambient weathering of magnesium oxide for CO₂ removal from air. *Nat. Commun.* 11 (1), 1–10. <https://doi.org/10.1038/s41467-020-16510-3>.
- Oskierski, H.C., Długogorski, B.Z., Jacobsen, G., 2013. Sequestration of atmospheric CO₂ in chrysotile mine tailings of the Woodsreef Asbestos Mine, Australia: quantitative mineralogy, isotopic fingerprinting and carbonation rates. *Chem. Geol.* 358, 156–169. <https://doi.org/10.1016/j.chemgeo.2013.09.001>.
- Park, A.H.A., Fan, L.S., 2004. CO₂ mineral sequestration: physically activated dissolution of serpentine and pH swing process. *Chem. Eng. Sci.* 59 (22–23), 5241–5247. <https://doi.org/10.1016/j.ces.2004.09.008>.
- Parkhurst, D.L., Appelo, C.A.J., 2013. Description of Input and Examples for PHREEQC Version 3—A Computer Program for Speciation, Batch-Reaction, One-Dimensional Transport, and Inverse Geochemical Calculations. Denver, Colorado.
- Pearson, A.R., Hartland, A., Frisia, S., Fox, B.R.S., 2020. Formation of calcite in the presence of dissolved organic matter: partitioning, fabrics and fluorescence. *Chem. Geol.* 539, 119492. <https://doi.org/10.1016/j.chemgeo.2020.119492>.
- Power, I.M., Harrison, A.L., Dipple, G.M., Wilson, S.A., Kelemen, P.B., Hitch, M., Southam, G., 2013. Carbon mineralization: from natural analogues to engineered systems. *Rev. Mineral. Geochem.* 77, 305–360. <https://doi.org/10.2138/rmg.2013.77.9>.
- Power, I.M., Kenward, P.A., Dipple, G.M., Raudsepp, M., 2017. Room temperature magnesite precipitation. *Cryst. Growth Des.* 17 (11), 5652–5659. <https://doi.org/10.1021/acs.cgd.7b00311>.
- Pronost, J., Beaudoin, G., Lemieux, J.M., Hébert, R., Constantin, M., Marcouiller, S., Klein, M., Duchesne, J., Molson, J.W., Larachi, F., Maldague, X., 2012. CO₂-depleted warm air venting from chrysotile milling waste (Thetford mines, Canada): evidence for in-situ carbon capture from the atmosphere. *Geology* 40 (3), 275–278. <https://doi.org/10.1130/G32583.1>.
- Qin, Y., Edwards, R., Tong, F., Mauzerall, D.L., 2017. Can switching from coal to shale gas bring net carbon reductions to China? *Environ. Sci. Technol.* 51 (5), 2554–2562. <https://doi.org/10.1021/acs.est.6b04072>.
- Ramseyer, K., Miano, T.M., D'Orazio, V., Wildberger, A., Wagner, T., Geister, J., 1997. Nature and origin of organic matter in carbonates from speleothems, marine cements and coral skeletons. *Org. Geochem.* 26, 361–378. [https://doi.org/10.1016/S0146-6380\(97\)00008-9](https://doi.org/10.1016/S0146-6380(97)00008-9).
- Renforth, P., 2019. The negative emission potential of alkaline materials. *Nat. Commun.* 10 (1), 1401. <https://doi.org/10.1038/s41467-019-09475-5>.
- Renforth, P., Manning, D.A.C., Lopez-Capel, E., 2009. Carbonate precipitation in artificial soils as a sink for atmospheric carbon dioxide. *Appl. Geochem.* 24, 1757–1764. <https://doi.org/10.1016/j.apgeochem.2009.05.005>.
- Renforth, P., Mayes, W.M., Jarvis, A.P., Burke, I.T., Manning, D.A.C., Gruij, K., 2012. Contaminant mobility and carbon sequestration downstream of the Ajka (Hungary) red mud spill: the effects of gypsum dosing. *Sci. Total Environ.* 421–422, 253–259. <https://doi.org/10.1016/j.scitotenv.2012.01.046>.
- Rietveld, H.M., 1969. A profile refinement method for nuclear and magnetic structures. *J. Appl. Crystallogr.* 2, 65–71.
- Rostron, B.J., Kelley, L.L., Kreis, L.K., Holmden, C., 2002. Economic potential of formation brines: interim results from the Saskatchewan brine sampling program; Summary of investigations. Saskatchewan Geological Survey, Saskatchewan Ind. Resour. Misc. 2, 29. Report 2002-4-2, Paper C-1.
- Ruiz-Agudo, E., Kudlacz, K., Putnis, C.V., Putnis, A., Rodriguez-Navarro, C., 2013. Dissolution and carbonation of portlandite [Ca(OH)₂] single crystals. *Environ. Sci. Technol.* 47 (19), 11342–11349. <https://doi.org/10.1021/es402061c>.
- Saldi, G.D., Jordan, G., Schott, J., Oelkers, E.H., 2009. Magnesite growth rates as a function of temperature and saturation state. *Geochem. Cosmochim. Acta* 73 (19), 5646–5657. <https://doi.org/10.1016/j.gca.2009.06.035>.
- Sanz-Pérez, E.S., Murdock, C.R., Didas, S.A., Jones, C.W., 2016. Direct capture of CO₂ from ambient air. *Chem. Rev.* 116 (19), 11840–11876. <https://doi.org/10.1021/acs.chemrev.6b00173>.
- Schilling, R.D., Krijgsman, P., 2006. Enhanced weathering: an effective and cheap tool to sequester CO₂. *Clim. Change* 74, 349–354. <https://doi.org/10.1007/s10584-005-3485-y>.
- Seifritz, W., 1990. CO₂ Disposal by means of silicates. *Nature* 345, 486. <https://doi.org/10.1038/345486b0>.
- Siriwardane, R.V., Stevens, R.W., 2009. Novel regenerable magnesium hydroxide sorbents for CO₂ capture at warm gas temperatures. *Ind. Eng. Chem. Res.* 48 (4), 2135–2141. <https://doi.org/10.1021/ie8011598>.
- Stringfellow, W.T., Domen, J.K., Camarillo, M.K., Sandelin, W.L., Borglin, S., 2014. Physical, chemical, and biological characteristics of compounds used in hydraulic fracturing. *J. Hazard Mater.* 275, 37–54. <https://doi.org/10.1016/j.jhazmat.2014.04.040>.
- Tuan, V.A., Lee, C.H., 2018. Preparation of rod-like MgO by simple precipitation method for CO₂ capture at ambient temperature. *Vietnam J. Chem.* 56 (2), 197–202.
- Turvey, C.C., Wilson, S.A., Hamilton, J.L., Tait, A.W., McCutcheon, J., Beinlich, A., Fallon, S.J., Dipple, G.M., Southam, G., 2018. Hydrocalcites and hydrated Mg-carbonates as carbon sinks in serpentinite mineral wastes from the Woodsreef chrysotile mine, New South Wales, Australia: CO₂ availability controls carbonate mineralogy and efficiency of CO₂ air capture in mine tailings. *Int. J. Greenh. Gas Control* 79, 38–60. <https://doi.org/10.1016/j.ijggc.2018.09.015>.
- U.S. EPA, U.S. Environmental Protection Agency, 2020. Summary of Input on Oil and Gas Extraction Wastewater Management Practices under the Clean Water Act. EPA-821-S19-001. <https://www.epa.gov/sites/production/files/2020-05/documents/oil-gas-final-report-2020.pdf>. (Accessed 15 October 2020).
- Weinrauch, A.M., Folkerts, E.J., Alessi, D.S., Goss, G.G., Blewett, T.A., 2021. Changes to hepatic nutrient dynamics and energetics in Rainbow Trout (*Oncorhynchus Mykiss*) following exposure to and recovery from hydraulic fracturing flowback and produced water. *Sci. Total Environ.* 764, 142893. <https://doi.org/10.1016/j.scitotenv.2020.142893>.
- Wilson, S.A., Raudsepp, M., Dipple, G.M., 2006. Verifying and quantifying carbon fixation in minerals from serpentine-rich mine tailings using the Rietveld method with X-ray powder diffraction data. *Am. Mineral.* 91 (8–9), 1331–1341. <https://doi.org/10.2138/am.2006.2058>.
- Wilson, S.A., Dipple, G.M., Power, I.M., Thom, J.M., Anderson, R.G., Raudsepp, M., Gabites, J.E., Southam, G., 2009. Carbon dioxide fixation within mine wastes of ultramafic-hosted ore deposits: examples from the Clinton Creek and Cassiar Chrysotile deposits. *Canada. Econ. Geol.* 104, 95–112. <https://doi.org/10.2113/gsecongeo.104.1.95>.
- Wilson, S.A., Barker, S.L.L., Dipple, G.M., Atudorei, V., 2010. Isotopic disequilibrium during uptake of atmospheric CO₂ into mine process waters: implications for CO₂ sequestration. *Environ. Sci. Technol.* 44, 9522–9529. <https://doi.org/10.1021/es1021125>.
- Wilson, S.A., Harrison, A.L., Dipple, G.M., Power, I.M., Barker, S.L.L., Mayer, K.U., Fallon, S.J., Raudsepp, M., Southam, G., 2014. Offsetting of CO₂ emissions by air capture into mine tailings at the Mount Keith Nickel Mine, Western Australia: rates,

- controls and prospects for carbon neutral mining. *Int. J. Greenh. Gas Control* 25, 121–140. <https://doi.org/10.1016/j.ijggc.2014.04.002>.
- Xi, F., Davis, S.J., Ciais, P., Crawford-Brown, D., Guan, D., Pade, C., Shi, T., Syddall, M., Lv, J., Ji, L., Bing, L., Wang, J., Wei, W., Yang, K.H., Lagerblad, B., Galan, I., Andrade, C., Zhang, Y., Liu, Z., 2016. Substantial global carbon uptake by cement carbonation. *Nat. Geosci.* 9 (12), 880–883. <https://doi.org/10.1038/ngeo2840>.
- Yadav, V.S., Prasad, M., Khan, J., Amritphale, S.S., Singh, M., Raju, C.B., 2010. Sequestration of carbon dioxide (CO₂) using red mud. *J. Hazard Mater.* 176 (1–3), 1044–1050. <https://doi.org/10.1016/j.jhazmat.2009.11.146>.
- Zhao, L., Sang, L., Chen, J., Ji, J., Teng, H.H., 2010. Aqueous carbonation of natural brucite: relevance to CO₂ sequestration. *Environ. Sci. Technol.* 44, 406–411. <https://doi.org/10.1021/es9017656>.
- Zhong, C., Li, J., Flynn, S.L., Nesbø, C.L., Sun, C., von Gunten, K., Lanoil, B.D., Goss, G.G., Martin, J.W., Alessi, D.S., 2019. Temporal changes in microbial community composition and geochemistry in flowback and produced water from the Duvernay formation. *ACS Earth Space Chem.* 3 (6), 1047–1057. <https://doi.org/10.1021/acsearthspacechem.9b00037>.
- Zhong, C., Zolfaghari, A., Hou, D., Goss, G.G., Lanoil, B.D., Gehman, J., Tsang, D.C.W., He, Y., 2021. Alessi, D. S. Comparison of the hydraulic fracturing water cycle in China and North America: a critical review. *Environ. Sci. Technol.* 55 (11), 7167–7185. <https://doi.org/10.1021/acs.est.0c06119>.
- Ziemkiewicz, P.F., He, Y.T., 2015. Evolution of water chemistry during Marcellus shale gas development: a case study in West Virginia. *Chemosphere* 134, 224–231. <https://doi.org/10.1016/j.chemosphere.2015.04.040>.
- Zolfaghari, A., Dehghanpour, H., Ghanbari, E., Bearinger, D., 2016a. Fracture characterization using flowback salt-concentration transient. *SPE J.* 21, 233–244. <https://doi.org/10.2118/168598-PA>.
- Zolfaghari, A., Dehghanpour, H., Noel, M., Bearinger, D., 2016b. Laboratory and field analysis of flowback water from gas shales. *J. Unconv. Oil Gas Resour.* 14, 113–127. <https://doi.org/10.1016/j.juogr.2016.03.004>.
- Zou, C., Ni, Y., Li, J., Kondash, A., Coyte, R., Lauer, N., Cui, H., Liao, F., Vengosh, A., 2018. The water footprint of hydraulic fracturing in Sichuan Basin, China. *Sci. Total Environ.* 630, 349–356. <https://doi.org/10.1016/j.scitotenv.2018.02.219>.